NANO LETTERS

Letter

pubs.acs.org/NanoLett

Large-Area (over 50 cm × 50 cm) Freestanding Films of Colloidal InP/ZnS Quantum Dots

Evren Mutlugun,[†,‡] Pedro Ludwig Hernandez-Martinez,[†,‡] Cuneyt Eroglu,[†] Yasemin Coskun,[†] Talha Erdem,[†] Vijay K. Sharma,[†] Emre Unal,[†] Subhendu K. Panda,[§] Stephen G. Hickey,[§] Nikolai Gaponik,[§] Alexander Eychmüller,[§] and Hilmi Volkan Demir*[,†,‡]

[†]Department of Physics, Department of Electrical and Electronics Engineering, and UNAM − Institute of Materials Science and Nanotechnology, Bilkent University, TR-06800, Ankara, Turkey

[‡]Luminous! Center of Excellence for Semiconductor Lighting and Displays, School of Electrical and Electronic Engineering, School of Mathematical and Physical Sciences, Nanyang Technological University, Nanyang Avenue, Singapore 639798, Singapore

[§]Physical Chemistry/Electrochemistry, TU Dresden, Bergstrasse 66b, 01062 Dresden, Germany

Supporting Information

ABSTRACT: We propose and demonstrate the fabrication of flexible, freestanding films of InP/ZnS quantum dots (QDs) using fatty acid ligands across very large areas (greater than 50 cm × 50 cm), which have been developed for remote phosphor applications in solid-state lighting. Embedded in a poly(methyl methacrylate) matrix, although the formation of stand−alone films using other QDs commonly capped with trioctylphosphine oxide (TOPO) and oleic acid is not efficient, employing myristic acid as ligand in the synthesis of these QDs, which imparts a strongly hydrophobic character to the thin film, enables film formation and ease of removal even on surprisingly large areas, thereby avoiding the need for ligand exchange. When pumped by a blue LED, these Cd-free QD films allow for high color rendering, warm white light generation with a color rendering index of 89.30 and a correlated color temperature of 2298 K. In the composite film, the temperature-dependent emission kinetics and energy transfer dynamics among different-sized InP/ZnS QDs are investigated and a model is proposed. High levels of energy transfer efficiency (up to 80%) and strong donor lifetime modification (from 18 to 4 ns) are achieved. The suppression of the nonradiative channels is observed when the hybrid film is cooled to cryogenic temperatures. The lifetime changes of the donor and acceptor InP/ZnS QDs in the film as a result of the energy transfer are explained well by our theoretical model based on the exciton−exciton interactions among the dots and are in excellent agreement with the experimental results. The understanding of these excitonic interactions is essential to facilitate improvements in the fabrication of photometrically high quality nanophosphors. The ability to make such large-area, flexible, freestanding Cd-free QD films pave the way for environmentally friendly phosphor applications including flexible, surface-emitting light engines.

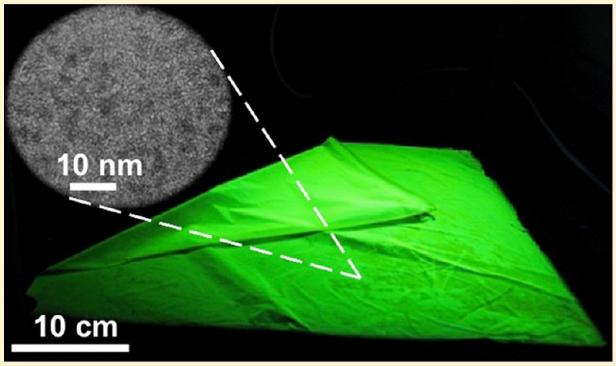

KEYWORDS: *Semiconductor quantum dots, large-area freestanding films, excitons, nonradiative energy transfer, white light generation, remote phosphors*

In the past few decades, semiconductor colloidal quantum dots (QDs), also known as nanocrystals, have attracted substantial interest for device applications including light-emitting diodes (LEDs) important for solid-state lighting.[1−3] The demand for these QD particles has risen as a result of their favorable electronic and optical properties. For example, their band gap engineering can be conveniently achieved by tuning the particle size, which has made semiconductor QDs versatile in device applications.[4,5] However, colloidal QDs are commonly synthesized in solution and the ability to transfer them from dispersion to solid form, for example, in polymeric host media, is essential from a typical device application point of view. To date, there have been previous reports on QD solids in polymer matrices. QDs, mostly type II−VI Cd based materials, have been extensively studied for their use in polymers in order to benefit from the advantageous properties of the polymers.[6−8] By incorporating them into a polymeric film, QDs gain elasticity and processability, which they cannot provide in their as-synthesized form.[9] However, solid film formation from these colloidal QDs in solution is challenging and requires a high level of understanding of the behavior of their complex mixtures in order to achieve films of high optical

Received: March 29, 2012
Revised: June 28, 2012
Published: July 11, 2012

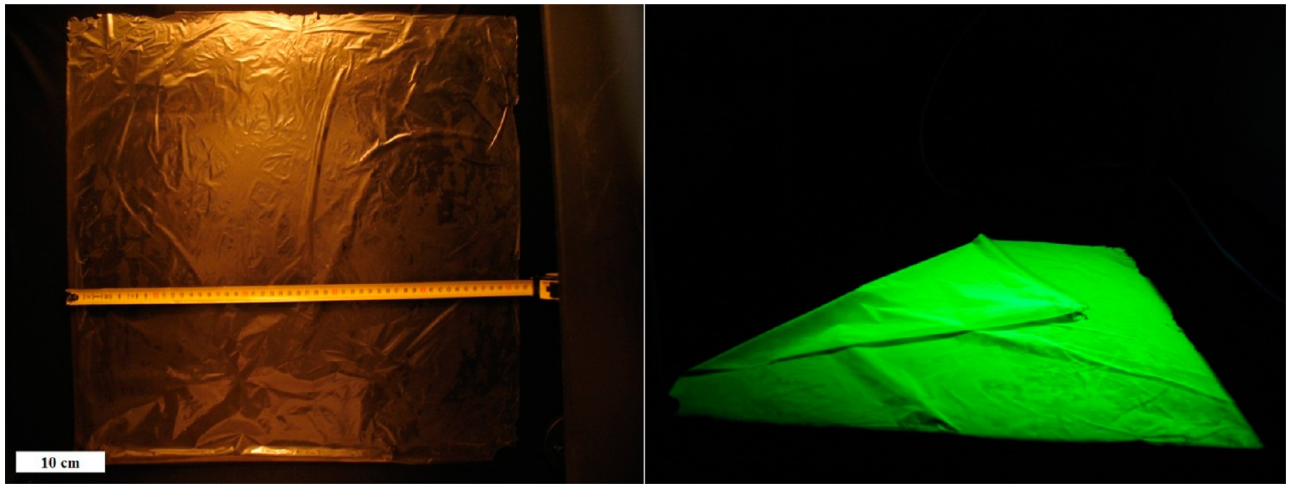

Figure 1. Photograph of a 51 cm × 51 cm InP/ZnS QD film under room light along with a ruler (left) and the folded film under UV illumination (right).

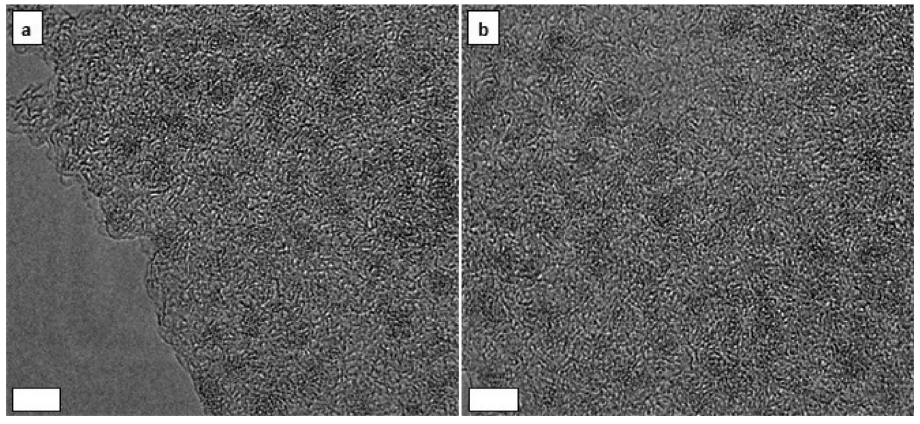

Figure 2. TEM images showing the distribution of InP/ZnS QDs in the PMMA matrix: (a) close to the edge of the film cross-section on the TEM grid and (b) an exemplary location at an inner point across the thickness of the cross-section, as is repeated at other locations (here the scale bar is 5 nm).

quality. The optimal QD film should be capable of standing alone, provide versatility, flexibility, and mechanical strength and be able to be fabricated over large areas. These requirements presently drive the strong research efforts into stand−alone flexible films of QDs.

Considering recent extensive research activities on large- area flexible electronics,[10] the implementation of QD-based large-area systems is highly desirable for use in matching large-area optoelectronic devices including light engines, displays, photovoltaics, and sensors. For this purpose, Tetsuka et al. reported flexible clay films of Cd-containing QDs.[11] In their study, although the proposed procedure was an interesting one, the films were small in size and required ligand exchange of the quantum dots and preparation of the clay suspension. In another study, Neves et al.,[8] flexible films containing CdSe/ZnS QDs within a sol−gel matrix were developed that were in the size range of a few centimeters. Previously, Zhang and colleagues also studied the use of functional polymers together with CdTe QDs for the formation of different geometrical shapes.[7] Their work further demonstrated the preparation of microspheres of QD-containing composites. However, again the resulting film sizes were limited. Although these previous reports have provided new techniques for the formation of QD−polymer composites, the literature is lacking a demonstration of freestanding QD solids of large area. Furthermore, from the ecological point of view, the use of Cd-free QDs such as those based on InP to enable eco-friendly applications to surpass the dominating Cd-based QD research activities is a hot topic.

Today while the research on Cd-based colloidal QDs (e.g., CdSe, CdTe, CdSe/CdS, and CdSe/ZnS) is quite mature with respect to their synthesis and applications,[12−18] recent research on In-based QDs has mainly focused on the synthesis methodology and understanding of the growth mechanisms and crystal structure of these materials.[19−25] Moreover, the use of In-based QDs for various applications has not been investigated except for a few reports that discuss lasing possibilities and imaging of cells.[26,27] Here we propose the use and demonstrate the manufacture of flexible, stand−alone, very large-area films of InP/ZnS QDs that hold the promise for high-end device applications. We study the emission kinetics and nonradiative energy transfer in the films and show high-quality white light generation by placing these films over a blue LED platform for remote phosphor applications.

Results and Discussion. In this work, InP/ZnS QDs are synthesized with fatty acid ligands in order to avoid the need for ligand exchange in the subsequent film formation process. The ligand, myristic acid, employed for the synthesis of these

dx.doi.org/10.1021/nl301198k | *Nano Lett.* 2012, 12, 3986−3993

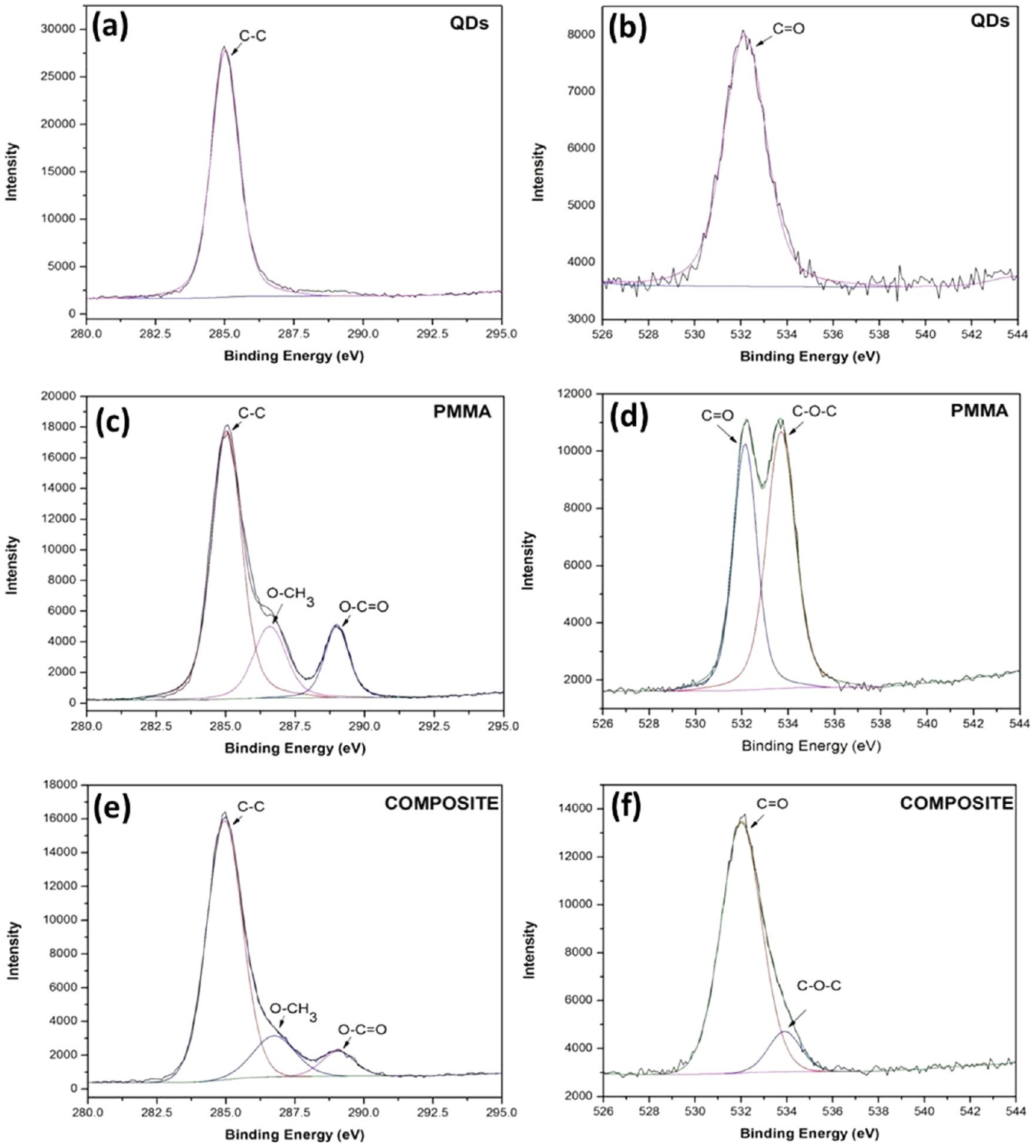

Figure 3. XPS spectra of the InP/ZnS quantum dot only (a) for carbon and (b) for oxygen analysis, XPS spectra of the PMMA only (c) for carbon and (d) for oxygen analysis and XPS spectra of the composite film (e) for carbon and (f) for oxygen analysis.

QDs, is a fatty acid that provides a good hydrophobic surface when incorporated into poly(methyl methacrylate) (PMMA) (see Supporting Information). This does not happen with Cd-containing QDs to the desired extent to enable one to achieve large-area stand−alone QD films. The InP/ZnS QDs dissolved in PMMA can be easily peeled off from the substrate after the solvent has fully evaporated (see Figure 1). Negative control experiments were performed using PMMA alone and also PMMA mixed with trioctylphosphine oxide (TOPO) and oleic acid capped QDs under the same conditions as the InP-based QDs. In these control experiments, even with such hydrophobic ligands it was found that neither of these films allowed for an easy peeling-off process that is required for the formation of uniform large-area freestanding films. The large-area, uniform film formation associated with the myristic acid

dx.doi.org/10.1021/nl301198k | *Nano Lett.* 2012, 12, 3986−3993

capped InP/ZnS QDs is a unique property, which opportunely enables large-area device applications.

In order to study the homogeneity and optical quality of the produced films, transmission electron microscopy (TEM) studies of slides prepared by microtome cross-sectional cutting of the QD loaded PMMA composites were undertaken. The details of the preparation of the microtome samples are given in Methods. The TEM images taken at various positions of the sample demonstrate the uniformity of the QDs dispersed within the host PMMA (see Figure 2). Furthermore, absorption measurements at various positions of the sample also verify the uniformity of the films, as presented in Figure S4 in the Supporting Information.

To characterize the elemental composition of the QD composite film, we undertook X-ray photoelectron spectroscopy (XPS) experiments. The high-resolution carbon 1s and oxygen 1s spectra are shown for the PMMA polymer, InP/ZnS QDs and the QD-PMMA composite in Figure 3. For PMMA, the C 1s spectra are resolved into three components with different bonding states: C−C at 285.0 eV, O−CH_3 at 286.5 eV, and O−C═O at 288.9 eV. O 1s spectra of the PMMA polymer consist of two components: C═O at 532.1 eV and C−O−C at 533.6 eV. The atomic percentage of the peaks are C−C (51.49%), O−CH_3 (15.12%), O−C═O (11.18%), C═O (9.79%), and C−O−C (12.42%), the distribution of which is common for standard XPS spectra of the PMMA.[28] High-resolution C 1s and O 1s spectra of QDs (due to ligands) show single peaks at 285.0 and 532.1 eV, respectively. The C 1s spectra of the composite PMMA-QD film are also resolved into three components and the O 1s spectra into two components, similar to pure PMMA. Here we observe modifications in the atomic percentages of the peaks in the composite verifying the incorporation of QDs in the composite. The atomic percentage of the peaks are C−C (58.58%), O−CH_3 (11.03%), O−C═O (5.26%), C═O (22.29%), and C−O−C (2.84%). We also observe a large decrease in the intensity of the C 1s peak of the pure QDs in the composite, which also suggests a change in the microenvironment of the QDs in the composite. This is further confirmed by the shift in the QD elemental peaks (0.3 eV) in the composites compared to the pure QDs (see Supporting Information).[29] The XPS results therefore support the notion that the QDs and PMMA form a composite structure.

To investigate the emission kinetics of the InP/ZnS QD films, we have studied Förster-type nonradiative energy transfer (FRET) within the film. The use of QDs as energy transfer agents for FRET-based applications has been previously studied extensively for other material systems with the view to developing new platforms for light generation and harvesting.[30−33] Although, such FRET-based systems have also been widely used in conjunction with dyes, proteins, and other nanostructured materials including quantum wells, quantum wires, and quantum dots,[34−41] FRET-based systems of QD-polymer composites for such free-standing forms have not been studied to date, which would introduce a new channel from the light generation and harvesting application point of view. In particular, our previous study demonstrated a possibility of efficient tuning of color coordinates of QDs/polymer composites via controllable FRET.[18] Figure 4 shows the emission and absorption spectra of green-emitting (donor) and red-emitting (acceptor) InP/ZnS QDs in solution together with their transmission electron microscopy (TEM) image in the inset. The diameter of these donor and acceptor QDs are observed from the TEM images to be ∼2.4 and 2.8 nm,

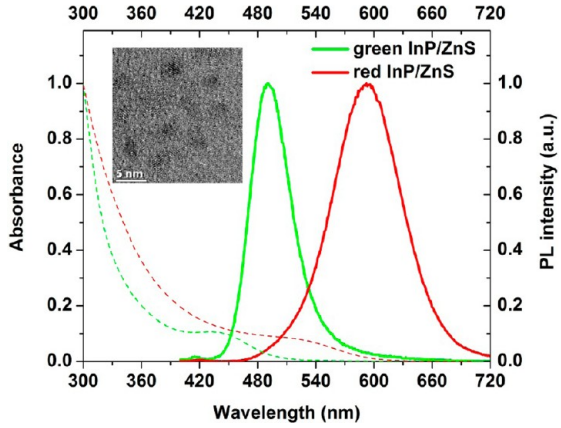

Figure 4. Normalized photoluminescence (solid line) and absorption (dashed line) spectra of the donor and acceptor InP/ZnS QDs. (inset) TEM image of the InP/ZnS QDs. The scale bar is 5 nm.

respectively. The acceptor QDs have been chosen to emit around 100 nm further to the red of the donor emission peak to prevent the emission overlap to a good extent and study their emission kinetics and the energy transfer between them.

The effect of the acceptor on the donor emission kinetics was studied by comparing the time-resolved photoluminescence (TRPL) decay profile of the bare donor QD containing film with the donor−acceptor QD film (with both samples having the same donor concentration) (see Supporting Information Figure S8). In the film, the peak emission wavelengths of the donor and acceptor QDs are 490 and 590 nm, respectively, and are therefore spectrally well-separated from each other (see also Figure 6), making the time-resolved analysis viable. The temperature dependence of the time-resolved fluorescence for each species of interest was also investigated and the decay curves were fit using a triexponential fitting function. The requirement for the use of triexponential functions for the fitting is due to the nontrivial emission kinetics of the InP/ZnS quantum dots. In various QD samples, the monoexponential decay originates mainly from radiative decay channels and one would expect this type of decay from high-quality QDs, that is, QDs that are mostly free of defects and surface trap states. In other words, the main contribution to the emission decay is the radiative recombination rate. On the other hand, a multi-exponential decay stems from the presence of nonradiative channels that are associated with energy transfer, Auger recombination/relaxation processes, and possibly defects and surface traps. Thus, the main contribution to the emission decay is from the nonradiative recombination rates. In such cases, the amplitude-weighted average lifetime gives a good estimate for the exciton lifetime, as has been suggested for the FRET-mediated lifetime modifications.[42] The fitting parameters for the amplitude weighted lifetime for the donor and acceptor before and after FRET is given on Supporting Information in Tables SIII−SVI.

The amplitude-weighted lifetime values for the donor only films range from 18.45 to 28.26 ns as the sample temperature is decreased from 300 to 30 K. As the donor only sample was cooled from room temperature to cryogenic temperatures (30 K), the photoluminescence decay curves were observed to possess a gentler slope, that is, the lifetime increased, which implies the inhibition of nonradiative recombination channels, due to the suppression of the phonon vibrations at cryogenic temperatures. The in-film PL intensity of the film donor and

dx.doi.org/10.1021/nl301198k | Nano Lett. 2012, 12, 3986−3993

acceptor QDs as a function of temperature is also provided in the Supporting Information Figure S10. In addition, we have compared the emission kinetics of the donor only film sample with the donor−acceptor hybrid film and observed a significant decrease in the lifetime of the donor QDs when in the presence of acceptors. In other words, the donor lifetime shortens as the donor transfers its excitation energy to an acceptor present in close proximity in the film. Another conclusion derived from the temperature-dependent lifetime measurements of the hybrid film is that, as the films are cooled to cryogenic temperatures, the nonradiative recombination channels are suppressed due to the suppression of the phononic vibrations. Therefore, the lifetime becomes longer as in the case of the donor only film. These results are shown in Supporting Information Figure S9 together with the temperature dependent lifetimes of the bare donor and hybrid film samples as insets, and are summarized in Supporting Information Table SI.

Using the modification of the donor lifetimes, the corresponding FRET efficiencies were calculated using

$$\eta = 1 - \frac{\tau_{DA}}{\tau_D} \tag{1}$$

where τ_{DA} is the lifetime of the donor in the presence of the acceptor and τ_D is the lifetime of the donor alone. We observe ~80% energy transfer efficiency (see Figure 5, and Supporting Information Table SI), which is in good agreement with our theoretical model based on exciton−exciton interaction (details of the theoretical approach is also given in the Supporting Information).

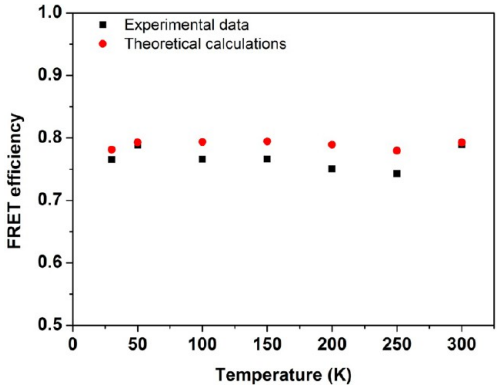

Figure 5. FRET efficiencies as a function of temperature: theoretical calculation (red circles) and experimental data (black squares).

In our theoretical approach, which is derived from the simplest rate model, the donor lifetime in the presence of the acceptor is given by

$$\tau_{DA}^{D} = \frac{\tau_{exc}^{D}}{1 + \left(\frac{R_0}{r}\right)^6} \tag{2}$$

where τ_{DA}^{D} is the donor exciton lifetime in the case of energy transfer. The energy transfer rate (γ_{trans}) between the donor−acceptor (D−A) QD pair is then obtained by

$$\gamma_{trans} = \frac{1}{\tau_D}\left(\frac{R_0}{r}\right)^6 \tag{3}$$

where R_0 is the Förster radius for the D−A pair and r is the separation distance for the D−A QD pair.[42] Supporting Information Table SI presents the experimentally measured and theoretically calculated lifetimes for the donor and acceptor pair when the measurements are analyzed at both the donor and acceptor emission wavelengths. Here the average separation distance (r) between the D−A pair is ~3.63 nm. In the theoretical analysis, we consider the temperature dependence using a semiempirical approach by calculating the change in the lifetime of the donor/acceptor species as a function of temperature (see inset Figure S8 and the Supporting Information). This is a valid approximation since the experimentally observed FRET efficiencies do not change significantly with changing temperature. To determine the number of quantum dots within the film, the TEM size of the donor and acceptor quantum dots, as well as the exctinction coefficients, were used. The total number of particles is calculated to be 5.05×10^{15}. Since the volume per unit particle is 2.77×10^{-25} m^3, in the film the particle-to-particle distance is found to be approximately 4.0 nm, which is less than the Förster radius and is also comparable to theoretically expected value of 3.63 nm. Also, the microtome TEM image of the film with a similar quantum dot loading shows the interparticle distance to be within the same distance range of <5 nm.

Figure 6 shows the photoluminescence spectra of the donor only and acceptor only films, together with the hybrid donor−acceptor film at room temperature, all under the same conditions. Here, as a result of FRET, the donor emission is suppressed by ~80% whereas the overall acceptor emission is increased by ~30%, which is obtained from the hybrid emission spectra (fit to the donor−acceptor emission in a Gaussian profile, as shown in the inset of Figure 6). We have also compared the results of the time-resolved measurements with the room temperature steady-state measurements. The modification of the steady-state photoluminescence of the donor and acceptor matches well that of the room temperature time-resolved lifetime modifications (79% for the donor and 57% for the acceptor). This implies that the excitons transferred from the donor are mostly contributed to the nearby acceptors.

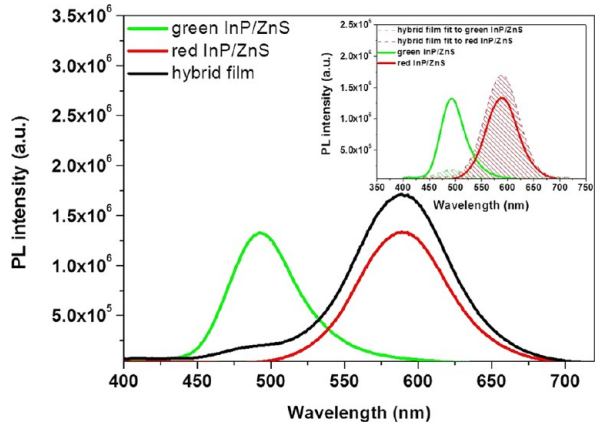

Figure 6. Steady-state room-temperature photoluminescence spectra of the films of the donor only, the acceptor only, and the hybrid film. The inset shows the same steady-state room-temperature photoluminescence spectra of the donor only, the acceptor only, and the hybrid film where the hybrid emission is fit to the donor and acceptor emissions as Gaussian curves.

Finally, as a proof-of-concept demonstration of the stand-alone films, InP/ZnS QD films were placed over a blue LED platform for high-quality white light generation. Previously,

dx.doi.org/10.1021/nl301198k | Nano Lett. 2012, 12, 3986−3993

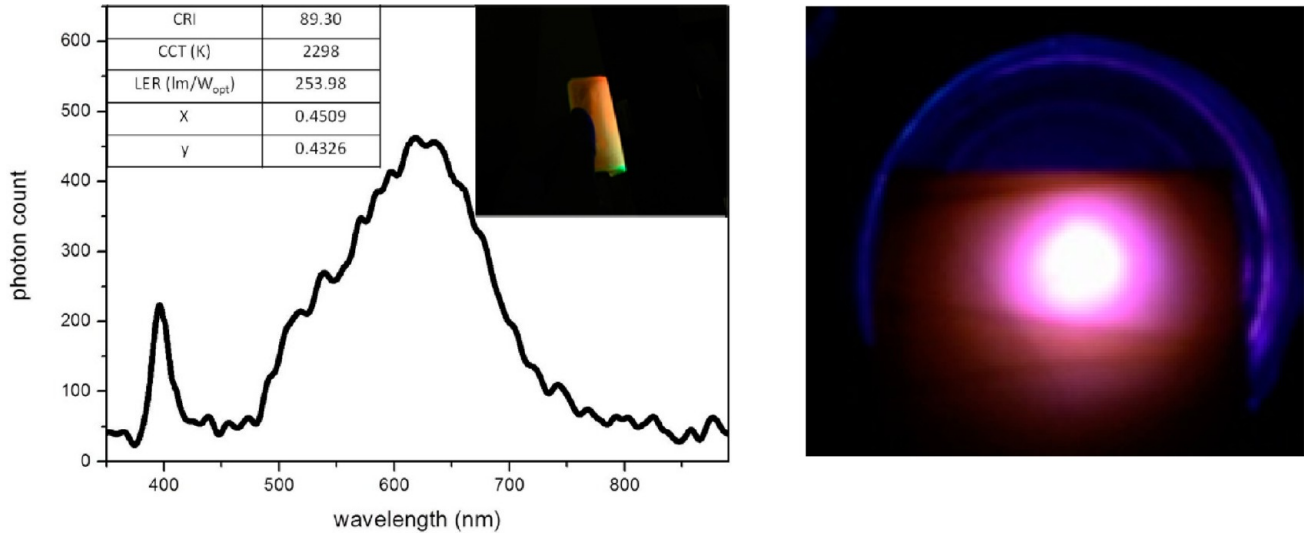

Figure 7. Electroluminescence spectra of a proof-of-concept white LED using an InP/ZnS QD film as the remote color-converting nanophosphors together with a blue LED chip (The bilayer film consisting of green and red QDs is shown in the inset). Also an exemplary device under operation is shown on the right.

Nann and co-workers[25] used green-emitting phosphors along with red-emitting InP/ZnS quantum dots. In this work, we present a white LED (WLED) in which both the red and green color components are provided by the green- and red-emitting InP/ZnS QDs forming a bilayer film, as shown in the inset of Figure 7, designed to result in high-photometric quality. Figure 7 shows the resulting emission spectra of the blue LED hybridized with the green−red emitting InP/ZnS quantum dot films and probed using a fiber coupled optical spectrum analyzer. The InGaN/GaN LED is driven at an electrical potential of 4.4 V. The white light generation using the excitation from the blue LED results in a color rendering index of 89.30 with a correlated color temperature of 2298 K and a luminous efficacy of optical radiation (LER) of 253.98 lm/W_{opt} and hence produces high color rendering, high spectral efficiency, and warm white light. We have not observed any changes in the spectra of the device under nonstop operation for >6 h indicating that no thermal stability issue was present under the operating conditions employed for the operation of the LED. These results demonstrate that these proof-of-concept WLED freestanding films are promising candidates for remote phosphor applications, potentially for high-temperature light engines.

In conclusion, we have demonstrated flexible, stand-alone films of InP/ZnS QD-polymer composites that were fabricated over very large areas of greater than 0.5 m × 0.5 m to enable high-end large-area optoelectronic applications. Here, as a potential next-generation light generation technology platform, we have also shown the use of these InP/ZnS QD films as remote color-converting nanophosphors for white LED applications. In these QD films, the theoretical results based on the exciton−exciton interaction model among the donor−acceptor QD pairs were also found to match well the experimental data. Given the ongoing extensive research efforts into large-area flexible electronics, the implementation of QD-based large-area systems is important for future large-area optoelectronic device applications including sensor arrays, solar conversion films, and large-area displays in addition to the surface-lighting platform demonstrated here. We believe that such very large-area Cd-free QD films, together with strong FRET processes that can be facilitated within them, open up new possibilities and hold great promise for innovative eco-friendly optoelectronics.

Methods. *Colloidal Synthesis of InP/ZnS QDs.* All reactions were performed under inert Ar atmosphere using a Schlenk line or glovebox. For the synthesis of the green-emitting donor InP/ZnS QDs, the procedure by Reiss and co-workers was followed.[24] In a typical one pot synthesis, 0.1 mmol indium myristate (prepared by dissolving indium acetate in myristic acid, In/MA: 1:4.3), 0.1 mmol zinc stearate, 0.1 mmol dodecanethiol, and 0.1 mmol tris(trimethylsilyl)-phosphine were dissolved in 8 mL of octadecene (ODE), mixed in a 3-necked 25 mL flask and evacuated at room temperature. The mixture was quickly heated to 300 °C under Ar or N_2 flow, and the growth of the QDs occurred within 20 min. Longer heating times resulted in a red shift of the emission peak. However, to achieve the orange/red-emitting acceptor QDs, a modified procedure proposed by the group of Nann[25] was used. For the core InP QDs, 0.1 mmol indium chloride, 0.1 mmol stearic acid, 0.08 mmol zinc undecylenate, and 0.2 mmol hexadecylamine were dissolved in 3 mL of ODE and heated to 240 °C under mixing in an inert atmosphere. At that temperature, the phosphor precursor (0.5 mL tris-(trimethylsilyl) phosphide dissolved in ODE, c = 0.2 mmol/mL) was injected and cooled to room temperature after the core growth was established at 220 °C for 20 min. For the shell growth, 0.3 mmol zinc undecylenate was mixed with the as-prepared core QDs and evacuated well before heating. The solution was then heated up to 220 °C and 1 mL of cyclohexyl isothiocyanate/ODE solution (c = 0.15 mmol/mL) was injected as the sulfur source followed by increasing the temperature to 240 °C and growth for 20 min, which resulted in orange/red-emitting QDs.

Fabrication of Large-Area Freestanding Films. As-synthesized InP/ZnS QDs were cleaned using isopropanol, acetone, and methanol extraction to remove the excess organic ligands and the precipitated particles were dissolved in fresh hexane/toluene.

Typically, 5 mL of PMMA A15 (MicroChem) is diluted with 5 mL of anisole and mixed with 4 mL of QDs in toluene with a

dx.doi.org/10.1021/nl301198k | *Nano Lett.* 2012, 12, 3986−3993

concentration of ca. 60 μM. The solution is stirred rigorously for 30 min, and the solution cleared from any air bubbles. Subsequently, 5 mL of this solution is drop-cast on a precleaned glass substrate with a ratio of 1 mL per 10 cm^2 of film. The glass substrate is placed on a smooth, uninclined plane to avoid nonuniformity of the film, and left for drying under controlled evaporation without the need for heating the substrate. Upon drying, the film is peeled off from the glass substrate, the thickness of the film prepared in this way being 65 μm. It is possible to tune the QD loading and thickness of the formed films by changing the ratio of the PMMA to anisole and the amount of QDs within the solution. The ease of peeling of the film was made possible because of the interaction of the ligand of the QDs, the myristic acid, with PMMA, thus providing a hydrophobic layer on the glass substrate that is readily peeled off. The contact angle measurements provided in the Supporting Information also confirmed that the resulting composite films were hydrophobic.

Preparation of the Microtome Slides for TEM Analysis. For the microtome cutting of cross sections of the InP/ZnS-PMMA film for the purpose of TEM analysis, a small amount of the film is put in the holder (capsules with a 5.6 mm O.D. and a pyramid tip, made from polyethylene) in which HistoResin (hardener) and Technovit 7100 were mixed in the ratio 1:15, respectively. The mixture is placed to one side for ~2 h to become solid. A Leica EM UC6/EM FC6 Ultramicrotome operated at −100 °C is used to slice the sample in thicknesses of up to ~100 nm. TEM images of ultrathin (~100 nm) sections of these films were recorded by FEI-Tecnai G2 F30 electron microscope operating at 300 kV.

Characterizations. A Cary 100 UV−vis, Cary Eclipse fluorescence spectrophotometer and Horiba Yvon Fluorolog were used for the optical characterizations of the QDs. The time-resolved fluorescence measurements were acquired with a Pico Quant Fluo Time 200 setup, TEM images were taken employing a FEI Tecnai G2 F30, and X-ray photoelectron spectroscopy (XPS) measurements using K-Alpha-Thermo. The mechanical characterizations were carried out with Instron 5969 MTS, the thermogravimetric analysis (TGA) was performed with a TGA Q500 (TA Instruments), the fluorescence microscopy images were taken using a Carl Zeiss Axio Scope upright microscope, and the contact angle measurements were taken with a Dataphysics OCA 15-EC.

■ ASSOCIATED CONTENT

Supporting Information

The chemical structure of the ligand and PMMA, the XPS measurement of the composite QD-PMMA film, the contact angle measurements and the mechanical characterization of the InP/ZnS QD composite films, a fluorescence microscopy image of the films, absorption measurements and TGA analysis of the produced films, TRPL analysis of the donor and acceptor species, donor and acceptor lifetime parameters, photoluminescence measurements of the donor and acceptor QDs as a function of temperature, and details of the theoretical section. This material is available free of charge via the Internet at http://pubs.acs.org.

■ AUTHOR INFORMATION

Corresponding Author

*E-mail: volkan@bilkent.edu.tr; hvdemir@ntu.edu.sg.

Notes

The authors declare no competing financial interest.

■ ACKNOWLEDGMENTS

This work is supported in part by NRF-CRP-6-2010-02 and NRF-RF-2009-09, in part by EU-FP7 Nanophotonics4Energy NoE, BMBF TUR 09/001, and TUBITAK EEEAG, 109E002, 109E004, 110E010, and 110E217. H.V.D. acknowledges support from ESF-EURYI and TUBA-GEBIP and E.M. acknowledges support from TUBITAK BIDEB. S.K.P. is grateful for a research fellowship provided by the Alexander von Humboldt Foundation.

■ REFERENCES

(1) Jang, E.; Jun, S.; Jang, H.; Lim, J.; Kim, B.; Kim, Y. White-light-emitting diodes with quantum dot color converters for display backlights. *Adv. Mater.* **2010**, *22*, 3076.

(2) Erdem, T.; Demir, H. V. Semiconductor Nanocrystals as Rare-Earth Alternatives. *Nat. Photonics* **2011**, *5*, 126.

(3) Panda, S. K.; Hickey, S. G.; Demir, H. V.; Eychmüller, A. Bright White-Light Emitting Manganese and Copper Co-Doped ZnSe Quantum Dots. *Angew. Chem., Int. Ed.* **2011**, 50.

(4) Konstantatos, G.; Howard, I.; Fischer, A.; Hoogland, S.; Clifford, J.; Klem, E.; Levina, L.; Sargent, E. H. Ultrasensitive Solution-Cast Quantum Dot Photodetectors. *Nature* **2006**, *442*, 180.

(5) Michalet, X.; Pinaud, F. F.; Bentolila, L. A; Tsay, J. M.; Doose, S.; Li, J. J.; Sundaresan, G.; Wu, A. M.; Gambhir, S. S.; Weiss, S. Quantum Dots for Live Cells, in Vivo Imaging, and Diagnostics. *Science* **2005**, *307*, 538.

(6) Lee, J.; Sundar, V. C.; Heine, J. R.; Bawendi, M. G.; Jensen, K. F. Full Color Emission from II−VI Semiconductor Quantum Dot−Polymer Composites. *Adv. Mater.* **2000**, *12*, 1102.

(7) Zhang, H.; Wang, C.; Li, M.; Zhang, J.; Lu, G.; Yang, B. Fluorescent Nanocrystal-Polymer Complexes with Flexible Processability. *Adv. Mater.* **2005**, *17*, 853.

(8) Neves, M. C.; Martins, M. A.; Soares-Santos, P. C. R.; Rauwel, P.; Ferreira, R. A. S; Monteiro, T.; Carlos, L. D.; Trindade, T. Photoluminescent, Transparent and Flexible Di-Ureasil Hybrids Containing CdSe/ZnS Quantum Dots. *Nanotechnology* **2008**, *19*, 155601.

(9) Xiong, H.-M.; Wang, Z.-D.; Liu, D.-P.; Chen, J.-S.; Wang, Y.-G.; Xia, Y.-Y. Bonding Polyether onto ZnO Nanoparticles: An Efficient Method for Preparing Polymer Nanocomposites with Tunable Luminescence and Stable Conductivity. *Adv. Funct. Mater.* **2005**, *15*, 1751.

(10) Rogers, J. A.; Bao, Z.; Baldwin, K.; Dodabalapur, A.; Crone, B.; Raju, V. R.; Kuck, V.; Katz, H.; Amundson, K.; Ewing, J.; Drzaic, P. Paper-Like Electronic Displays: Large-Area Rubber Stamped Plastic Sheets of Electronics and Microencapsulated Electrophoretic Inks. *Proc. Natl. Acad. Sci. U.S.A.* **2001**, *98*, 4835.

(11) Tetsuka, H.; Ebina, T.; Mizukami, F. Highly Luminescent Flexible Quantum Dot−Clay Films. *Adv. Mater.* **2008**, *20*, 3039.

(12) Yang, Y. A.; Wu, H.; Williams, K. R.; Cao, Y. C. Synthesis of CdSe and CdTe Nanocrystals without Precursor Injection. *Angew. Chem., Int. Ed.* **2005**, *117*, 6870.

(13) Peng, Z. A; Peng, X. Formation of High-Quality CdTe, CdSe, and CdS Nanocrystals Using CdO as Precursor. *J. Am. Chem. Soc.* **2001**, *123*, 183.

(14) Manna, L.; Scher, E. C.; Alivisatos, A. P. Synthesis of Soluble and Processable Rod-, Arrow-, Teardrop-, and Tetrapod-Shaped CdSe Nanocrystals. *J. Am. Chem. Soc.* **2000**, *122*, 12700.

(15) Gaponik, N.; Talapin, D. V.; Rogach, A. L.; Hoppe, K.; Shevchenko, E. V.; Kornowski, A.; Eychmüller, A.; Weller, H. Thiol-Capping of CdTe Nanocrystals: An Alternative to Organometallic Synthetic Routes. *J. Phys. Chem. B* **2002**, *106*, 7177.

(16) Dabbousi, B. O.; Rodriguez-Viejo, J.; Mikulec, F. V.; Heine, J. R.; Mattoussi, H.; Ober, R.; Jensen, K. F.; Bawendi, M. G. (CdSe)ZnS

Core-Shell Quantum Dots: Synthesis and Characterization of a Size Series of Highly Luminescent Nanocrystallites. *J. Phys. Chem. B* **1997**, *101*, 9463.
(17) Demir, H. V.; Nizamoglu, S.; Erdem, T.; Mutlugun, E.; Gaponik, N.; Eychmüller, A. Quantum dot integrated LEDs using photonic and excitonic color conversion. *Nano Today* **2011**, *6*, 632.
(18) Cicek, N.; Nizamoglu, S.; Ozel, T.; Mutlugun, E.; Karatay, D. U.; Lesnyak, V.; Otto, T.; Gaponik, N.; Eychmüller, A.; Demir, H. V. Structural tuning of color chromaticity through nonradiative energy transfer by interspacing CdTe nanocrystal monolayers. *Appl. Phys. Lett.* **2009**, *94*, 061105.
(19) Ryu, E.; Kim, S.; Jang, E.; Jun, S.; Jang, H.; Kim, B.; Kim, S.-W. Step-Wise Synthesis of InP/ZnS Core-Shell Quantum Dots and the Role of Zinc Acetate. *Chem. Mater.* **2009**, *21*, 2425.
(20) Xie, R.; Battaglia, D.; Peng, X. Colloidal InP Nanocrystals as Efficient Emitters Covering Blue to Near-Infrared. *J. Am. Chem. Soc.* **2007**, *129*, 15432.
(21) Thuy, U. T. D.; Thuy, P. T.; Liem, N. Q.; Li, L.; Reiss, P. Comparative Photoluminescence Study of Close-Packed and Colloidal InP/ZnS Quantum Dots. *Appl. Phys. Lett.* **2010**, *96*, 073102.
(22) Pham, T. T.; Tran, T. K. C.; Nguyen, Q. L. Temperature-Dependent Photoluminescence Study of InP/ZnS Quantum Dots. *Adv. Nat. Sci.: Nanosci. Nanotechnol.* **2011**, *2*, 025001.
(23) Thuy, U. T. D.; Reiss, P.; Liem, N. Q. Luminescence Properties of In(Zn)P Alloy Core/ZnS Shell Quantum Dots. *Appl. Phys. Lett.* **2010**, *97*, 193104.
(24) Li, L.; Reiss, P. One-pot Synthesis of Highly Luminescent InP/ZnS Nanocrystals without Precursor Injection. *J. Am. Chem. Soc.* **2008**, *130*, 11588.
(25) Ziegler, J.; Xu, S.; Kucur, E.; Meister, F.; Batentschuk, M.; Gindele, F.; Nann, T. Silica-Coated InP/ZnS Nanocrystals as Converter Material in White LEDs. *Adv. Mater.* **2008**, *20*, 4068.
(26) Gao, S.; Zhang, C.; Liu, Y.; Su, H.; Wei, L.; Huang, T.; Dellas, N.; Shang, S.; Mohney, S. E.; Wang, J.; Xu, J. Lasing from Colloidal InP/ZnS Quantum Dots. *Opt. Exp.* **2011**, *19*, 5528.
(27) Yong, K.-T.; Ding, H.; Roy, I.; Law, W.-C.; Bergey, E. J.; Maitra, A.; Prasad, P. N. Imaging Pancreatic Cancer Using Bioconjugated InP Quantum Dots. *ACS Nano* **2009**, *3*, 502.
(28) Rosencrance, S. W.; Way, W. K.; Winograd, N; Shirley, D. A. Polymethylmethacrylate by XPS. *Surf. Sci. Spectra* **2008**, *2*, 71.
(29) Chen, W. Y.; Ghule, A. V.; Chang, J. Y.; Chen, B. Y.; Liu, J. Y.; Tzing, S. H.; Ling, Y. C. Synthesis, Characterization, Photo and Physicochemical Properties of 11-Mercaptoundecanoic Acid and Tetraaniline Capped CdS Quantum Dots. *Mater. Chem. Phys.* **2010**, *123*, 742.
(30) Mutlugun, E.; Samarskaya, O.; Ozel, T.; Cicek, N.; Gaponik, N.; Eychmüller, A.; Demir, H. V. Highly Efficient Nonradiative Energy Transfer Mediated Light Harvesting in Water Using Aqueous CdTe Quantum Dot Antennas. *Opt. Exp.* **2010**, *18*, 10720.
(31) Medintz, I. L.; Mattoussi, H. Quantum Dot-Based Resonance Energy Transfer and Its Growing Application in Biology. *Phys. Chem. Chem. Phys.* **2009**, *11*, 17.
(32) Boeneman, K.; Mei, B. C.; Dennis, A. M.; Bao, G.; Deschamps, J. R.; Mattoussi, H.; Medintz, I. L. Sensing Caspase 3 Activity with Quantum Dot-Fluorescent Protein Assemblies. *J. Am. Chem. Soc.* **2009**, *131*, 3828.
(33) Freeman, R.; Finder, T.; Gill, R.; Willner, I. Probing Protein Kinase (CK2) and Alkaline Phosphatase with CdSe/ZnS Quantum Dots. *Nano Lett.* **2010**, *10*, 2192.
(34) Clapp, A. R.; Medintz, I. L.; Mattoussi, H. Förster Resonance Energy Transfer Investigations Using Quantum-Dot Fluorophores. *Chem. Phys. Chem.* **2006**, *7*, 47.
(35) Higgins, C.; Lunz, M.; Bradley, A. L.; Gerard, V. A; Byrne, S.; Gunko, Y. K.; Lesnyak, V.; Gaponik, N. Energy Transfer in Colloidal CdTe Quantum Dot Nanoclusters. *Opt. Express* **2010**, *18*, 24486.
(36) Franzl, T.; Koktysh, D. S.; Klar, T. A.; Rogach, A. L.; Feldmann, J.; Gaponik, N. Fast Energy Transfer in Layer-by-Layer Assembled CdTe Nanocrystal Bilayers. *Appl. Phys. Lett.* **2004**, *84*, 2904.
(37) Clapp, A. R.; Medintz, I. L.; Mauro, J. M.; Fisher, B. R.; Bawendi, M. G.; Mattoussi, H. Fluorescence Resonance Energy Transfer Between Quantum Dot Donors and Dye-Labeled Protein Acceptors. *J. Am. Chem. Soc.* **2004**, 301.
(38) Lee, J.; Govorov, A. O.; Kotov, N. A. Bioconjugated Superstructures of CdTe Nanowires and Nanoparticles: Multistep Cascade Forster Resonance Energy Transfer and Energy Channeling. *Nano Lett.* **2005**, *5*, 2063.
(39) Willard, D. M.; Carillo, L. L.; Jung, J.; Van Orden, A. CdSe-ZnS Quantum Dots as Resonance Energy Transfer Donors in a Model Protein-Protein Binding Assay. *Nano Lett.* **2001**, *1*, 581.
(40) Medintz, I. L.; Clapp, A. R.; Mattoussi, H.; Goldman, E. R.; Fisher, B.; Mauro, J. M. Self-Assembled Nanoscale Biosensors Based on Quantum Dot FRET Donors. *Nat. Mat.* **2003**, *2*, 630.
(41) Wargnier, R.; Baranov, A. V.; Maslov, V. G.; Stsiapura, V.; Artemyev, M.; Pluot, M.; Sukhanova, A.; Nabiev, I. Energy Transfer in Aqueous Solutions of Oppositely Charged CdSe/ZnS Core/Shell Quantum Dots and in Quantum Dot-Nanogold Assemblies. *Nano Lett.* **2004**, *4*, 451.
(42) Lakowicz, J. R. *Principles of fluorescence spectroscopy*; Springer: New York, 2006.